

# Models of Electrostatically Fringe Field Actuated MEMS Resonators: Voltage-Amplitude Response of Parametric Resonance

University of Texas Rio Grande Valley, Edinburg, TX 78539, USA dumitru.caruntu@utrgv.edu

**Abstract.** This paper deals with the voltage-amplitude response of parametric resonance of micro-electromechanical system (MEMS) cantilever beam resonators actuated solely by fringing electrostatic fields. The system comprises a micro cantilever beam positioned parallel to a ground plate, connected via an AC voltage source which leads to electrostatic actuation. The ground plate has a hole allowing the cantilever beam deflections larger than the gap and therefore eliminating the pull-in phenomenon. A fringing field capacitance model (based on Sakurai's empirical formula) is used in this work and compared to a more traditional fringing field model based on Palmer's formula. The fringing field is the electric field between the ground plate and the beam's top and sidewalls. In both models, due to the configuration of the ground plate with a hole, the parallel-plate capacitance is removed, so only the fringe field actuation is considered. For parametric resonance, the AC voltage frequency is near the resonator's natural frequency. A nondimensionalized partial differential equation governing the system is reduced to a single-mode Reduced Order Model (ROM), which is then analytically solved using the Method of Multiple Scales (MMS). The resulting voltage-amplitude bifurcation diagram reveals a trivial solution and two branches, one stable and one unstable, emerging from super- and subcritical bifurcation points. A twomode ROM is also developed and solved numerically to verify these findings, and the resulting equations are implemented in AUTO-07p (a continuation and bifurcation analysis software) to obtain further voltage response data. Fringing field capacitance model predictions are compared against fringing field model based on Palmer's formula predictions, and against the case of ground plate with no hole modeled by Palmer's formula.

**Keywords:** MEMS cantilever  $\cdot$  Fringe-field actuation  $\cdot$  Voltage-amplitude response

#### 1 Introduction

Micro-electromechanical Systems (MEMS) technologies enable the creation of structures, systems, and devices at the micron scale [1]. At their core, MEMS integrate mechanical microstructures, microsensors, microactuators, and microelectronics onto

a single silicon chip. Due to their low production cost, compact size, minimal power consumption, adaptable geometry, and application-specific functionality, MEMS have become a preferred alternative to traditional sensors and actuators [2]. Various actuation methods are used in MEMS devices, including electrostatic, electrothermal, electromagnetic, and piezoelectric techniques. Among these, electrostatic actuation is widely favored for its simple design, fast response time, and ease of fabrication [3], though it presents challenges such as high driving voltages and significant nonlinearities. A deep understanding of the nonlinear dynamic response of MEMS is crucial for the development and precise control of novel devices.

The MEMS field has grown significantly, with potential applications across diverse industries [4]. MEMS are now widely used in biomedical, automotive, defense, communications, and aerospace domains. In particular, the field of biomedical MEMS (bioMEMS) has advanced considerably through the integration of MEMS technology and biological sciences. This integration has enabled the development of biosensors, diagnostic tools, drug delivery systems, and surgical instruments [5]. One application is the dynamic-mode cantilever biosensor, used to detect pathogens by measuring shifts in resonant frequency due to mass loading from attached bacteria or viruses [6]. These sensors can measure cell mass with high sensitivity and monitor bacterial growth. For instance, Ilic et al. [7] demonstrated the detection and quantification of E. coli using a dynamic-mode cantilever sensor, and this approach has since been adopted in multiple studies for rapid bacterial detection [6].

Electrostatic actuation primarily results from the electric field between two oppositely charged parallel plates, creating an attractive force [3]. This system includes a flexible cantilever beam and a conductive ground plate, with a dielectric medium filling the gap g between them. The electrostatic force  $F_e$  exerted on the cantilever beam is

$$F_e = \frac{1}{2} \frac{\partial C}{\partial g} V_0^2 \tag{1}$$

where C is the capacitance and  $V_0$  is the excitation voltage. For a rectangular cross-section, capacitance depends on the beam's length l, width W, the gap g, and the dielectric constant  $\varepsilon_r$  of the medium [8]. As the beam deflects toward the ground plate, the gap changes, altering the capacitance. When the applied voltage exceeds a critical threshold, in the case of ground plate with no hole, pull-in instability may occur, causing the beam to collapse, one of the most significant nonlinear phenomena in electrostatic MEMS devices [9].

Accurately modeling fringing capacitance between two conductors has long been a focus in the Very Large-Scale Integration (VLSI) community [10]. While fringing effects are minor in wide beams, they become significant in narrow-beam geometries [11]. Fringe-actuated MEMS devices have demonstrated practical applications [8, 11, 12]. Van der Meijs and Fokkema [10] reported the difference between traditional parallel-plate capacitance  $C_{pp}$  and fringing capacitances, where the electric field extends to the top and side walls of the cantilever. The fringing capacitances  $C_1$  and  $C_4$  are between resonator's top surface and the ground plate, and  $C_2$  and  $C_3$  between resonator's sides and the ground plate, in a 2D system. Chang [13] developed an accurate, but mathematically complex, formula using conformal mapping techniques to account for these effects. To

simplify modeling, empirical capacitance formulas such as Sakurai and Tamaru [14] have been proposed.

This paper employs Sakurai and Tamaru [14] empirical capacitance formula, which includes contributions from fringe fields acting on the top and sidewalls of the cantilever, to investigate the voltage—amplitude response of parametric resonance of fringe-actuated MEMS cantilever beams parallel to a ground plate with a hole. The Method of Multiple Scales (MMS) and a two-term Reduced Order Model (2T ROM) are used.

In parametric resonance [15], the frequency of the AC voltage is near the beam's first natural frequency. However, the actuation force operates at twice that frequency. Both MMS and 2T ROM are used to predict bifurcation points of the voltage–amplitude response. The results from both models, fringing capacitance model based on Ref. [14] and fringing model based on Palmer's formula, are compared and discussed. MMS aligns well with ROM at small amplitudes. However, MMS fails to capture instabilities seen at higher amplitudes.

# 2 Equation of Motion

Figure 1 shows a flexible MEMS cantilever beam positioned above a fixed ground plate with a rectangular hole that allows deflections beyond the gap distance. When an AC voltage is applied between the two electrodes, a fringing electrostatic force is generated, inducing vibration in the beam. The dimensionless partial differential equation of motion for the cantilever beam based on the capacitance model, along with the corresponding boundary conditions, are

$$\frac{\partial^2 u}{\partial \tau^2} + \frac{\partial^4 u}{\partial z^4} + b^* \frac{\partial u}{\partial \tau} = \frac{0.15\delta}{(1-u)^2} V^2 + \frac{C_f f^* \delta}{(1-u)^{(11/9)}} V^2$$
 (2)

$$u(\tau,0) = \frac{\partial u}{\partial z}(\tau,0) = \frac{\partial^2 u}{\partial z^2}(\tau,1) = \frac{\partial^3 u}{\partial z^3}(\tau,1) = 0$$
 (3)

where the dimensionless variables and parameters are as follows: u is the beam's deflection,  $\tau$  time, z longitudinal coordinate,  $b^*$  damping parameter,  $\delta$  voltage parameter, V voltage,  $C_f$  capacitance constant, and  $f^*$  capacitance fringe parameter. Note that the first term on the right-hand side of Eq. (2) results from  $\frac{1.15\delta}{(1-u)^2}V^2$ , Sakurai and Tamaru [14], from which  $\frac{\delta}{(1-u)^2}V^2$ , that is the term resulting from the electric field directly between the resonator and the ground plate, has been removed in order to model the fringe actuation in the case of ground plate with a hole. Table 1 shows the dimensional and dimensionless variables/parameters/constants. The empirical formula [14] used to describe the 2-D line capacitance that considers fringe contributions from the top and side walls of the beam is given by

$$\frac{C_1}{\varepsilon_o \varepsilon_r} = 1.15 \left(\frac{W}{g}\right) + 2.80 \left(\frac{h}{g}\right)^{2/9} \tag{4}$$

where  $C_1$  is the capacitance per unit length,  $\varepsilon_r$  is a dielectric constant,  $\varepsilon_0$  permittivity of free space, W beam width, h beam thickness, and g initial gap distance.

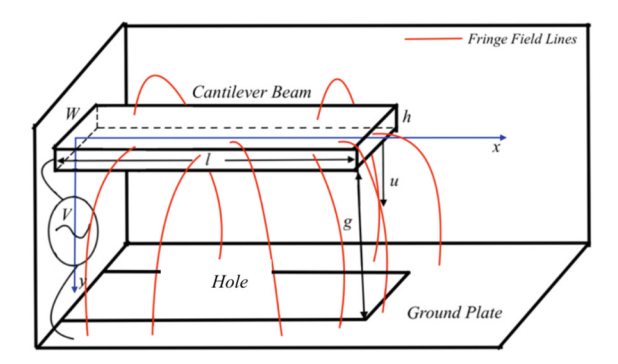


Fig. 1. Fringe field electrostatically actuated MEMS cantilever resonator

For this formula, the relative error is within 6% for 0.3 < W/g < 30 and 0.3 < h/g < 30. The first term of Eq. (4) can be considered as contributions from lower and upper surfaces, while the second term represents the side wall contribution [14]. Dimensionless variables/parameters, Eq. (2), are

$$u = \frac{w}{g}, z = \frac{x}{l}, \tau = \frac{t}{l^2} \sqrt{\frac{EI_0}{\rho A_0}}$$
 (5)

$$b^* = b \frac{l^2}{\sqrt{\rho A_0 E I_0}}, f = \frac{0.65g}{W}, f^* = \frac{h^{2/9}}{Wg^{-7/9}}, \delta = \frac{\varepsilon_0 W l^4}{2g^3 E I_0} V_0^2, \Omega^* = \Omega l^2 \sqrt{\frac{\rho A_0}{E I_0}}$$
(6)

where the dimensionless parameter f is the fringe parameter of the fringe model based on Palmer's formula [16], and  $\Omega^*$  dimensionless AC frequency. The dimensional variables, parameters and constants are as follows: w deflection, t time, x longitudinal coordinate, l beam length, l0 beam cross-section area, l10 beam cross-section moment of inertia, l21 damping coefficient, l22 material density, E Young's modulus, l32 AC frequency, and l33 voltage amplitude.

#### 3 Parametric Resonance

The dimensionless AC frequency,  $\Omega^*$ , is defined as a function of the natural frequency  $\omega_k$ , the detuning frequency  $\sigma$ , and a small bookkeeping parameter  $\varepsilon$  (used in the method of multiple scales, MMS). During parametric resonance,  $\Omega^*$  is close to the natural frequency of the cantilever beam ( $\Omega^* \approx \omega_k$ )

$$\Omega^* = \omega_k + \varepsilon \sigma \tag{7}$$

where the k-th dimensionless natural frequency is  $\omega_k = \overline{\omega}_k l^2 \sqrt{\rho A_0/EI_0}$ , and  $\overline{\omega}_k$  is the corresponding dimensional frequency. The detuning frequency  $\sigma$  represents the difference between the AC frequency and the natural frequency. The dimensionless voltage and voltage square used in this research are given by

$$V(\tau) = \cos\Omega^* \tau, V^2 = \frac{1}{2} + \frac{1}{4} \left( e^{2i\Omega^* t} + e^{-2i\Omega^* t} \right)$$
 (8)

One can notice from Eqs. (2) and (8) that the fringe electrostatic force has a frequency near twice the first natural frequency of the beam, resulting in parametric resonance.

# 4 Method of Multiple Scales

The Method of Multiple Scales (MMS) is a perturbation method. Both forcing terms at the right-hand side of Eq. (2) are expanded in Taylor series, retaining terms up to the third and fifth powers. Terms accompanied by the bookkeeping parameter  $\varepsilon$  are small terms indicating soft actuation and weak damping [16] in the system

$$\frac{\partial^2 u}{\partial \tau^2} + \frac{\partial^4 u}{\partial \tau^4} + \varepsilon b^* \frac{\partial u}{\partial \tau} = 0.15 \varepsilon \delta V^2 \left( 1 + 2u + 3u^2 + 4u^3 \right) + C_f \varepsilon f^* \delta V^2 (1 + \psi_1 u + \psi_2 u^2 + \psi_3 u^3) \tag{9}$$

Constant  $C_f$  is obtained from the empirical capacitance formula in [14], while  $\psi_k$  are constant coefficients derived from the Taylor expansion of  $1/(1-u)^{(11/9)}$ , which appears in the differential equation of motion Eq. 2. The time derivatives are given by

$$\frac{\partial}{\partial \tau} = D_0 + \varepsilon D_1, \quad \frac{\partial^2}{\partial \tau^2} = D_0^2 + 2\varepsilon D_0 D_1 + \varepsilon^2 D_1^2 \tag{10}$$

where  $T_0 = t$  is the fast time scale and  $T_1 = \varepsilon t$  is the slow time scale. The derivatives with respect to  $T_0$  and  $T_1$  are denoted by  $D_0$  and  $D_1$ , respectively. The uniform expansion of  $u(\tau, z)$  is considered as follows

$$u = u_0 + \varepsilon u_1$$
, and  $u^{(4)} = u_0^{(4)} + \varepsilon u_1^{(4)}$  (11)

Substitute Eqs. (10) and (11) into Eq. (9). Based on the powers of the bookkeeping parameter  $\varepsilon$ , two problems, namely the zeroth- and first-order, result as follows

$$\varepsilon^0: D_0^2 u_0 + u_0^{(4)} = 0 (12)$$

$$\varepsilon^{1}: D_{0}^{2}u_{1} + u_{1}^{(4)} = -2D_{0}D_{1}u_{0} - b^{*}D_{0}u_{0} + 0.15\delta V^{2} \left(1 + 2u_{0} + 3u_{0}^{2} + 4u_{0}^{3}\right) + C_{f}f^{*}\delta V^{2} (1 + \psi_{1}u_{0} + \psi_{2}u_{0}^{2} + \psi_{3}u_{0}^{3})$$

$$\tag{13}$$

The solution of the zeroth-order problem Eq. (12) is given by [17]:

$$u_0 = \phi(z)[A(T_1)e^{i\omega_k T_0} + \overline{A}(T_1)e^{-i\omega_k T_0}]$$
(14)

By substituting Eq. (14) into Eq. (13), the secular terms (terms proportional to  $e^{i\omega_0 T_0}$ ) are collected, and their sum is set to zero. Complex amplitude A and its conjugate  $\overline{A}$  are

$$A = \frac{1}{2} a_k e^{i\beta_k} \& \overline{A} = \frac{1}{2} a_k e^{-i\beta_k}$$

$$\tag{15}$$

where  $a_k$  and  $\beta_k$  are real amplitude and real phase, respectively. Once Eq. (15) is applied in the secular terms equation, the resulting equation is divided by  $e^{i\beta_k}$ . Denoting

$$\gamma = \sigma T_1 - \beta_k \tag{16}$$

both, the real and imaginary components of the secular terms' equation are separated and set equal to zero. The derivatives with respect to the slow scale  $T_1$  of amplitude a, and phase difference  $\gamma$ , are equated to zero to obtain the steady-state solutions as

$$a\sigma\omega_k g_2 + \frac{\delta ag_2}{8} \left(\frac{3}{10} + C_f f^* \psi_1\right) (2 + \cos 2\gamma) + \frac{\delta a^3 g_4}{16} \left(\frac{3}{10} + C_f f^* \psi_3\right) (3 + 2\cos 2\gamma) = 0 \tag{17}$$

$$-\frac{1}{2}b^*\omega_k ag_2 + \frac{1}{8}\delta ag_2 \sin 2\gamma \left(\frac{3}{10} + C_f f^* \psi_1\right) + \frac{1}{16}\delta a^3 g_4 \sin 2\gamma \left(\frac{3}{5} + C_f f^* \psi_3\right) = 0$$
(18)

It is important to note that these equations are satisfied by the trivial solution a = 0. Furthermore, a non-trivial solution is given by

$$a = \sqrt{\frac{8b^*\omega_1 g_2 - 2\delta g_2 \sin 2\gamma \left[ (3/10) + C_f f^* \psi_1 \right]}{\delta g_4 \sin 2\gamma \left[ (3/5) + C_f f^* \psi_3 \right]}}, \ \delta = \frac{80\omega_1 \left[ (3/2)b^* + b^* \cos 2\gamma + \sigma \sin 2\gamma \right]}{\left( 3\sin 2\gamma + 10C_f f^* \psi_1 \sin 2\gamma \right) (1 + \cos 2\gamma)}$$
(19)

where  $g_2 = \int_0^1 \phi_1^2 dz$ ,  $g_4 = \int_0^1 \phi_1^4 dz$ .

## 5 Reduced Order Model

A Reduced Order Model (ROM) using two modes of vibration (two terms) is developed using the first two mode shapes of a cantilever beam in order to obtain steady-state solutions. With enough terms, this technique is considered accurate for capturing both weak and strong nonlinearities, as well as small and large amplitude responses [16]. The dimensionless deflection u in Eq. (2) is considered as follows

$$u(\tau, z) = \sum_{i=1}^{N} u_i(\tau)\phi_i(z)$$
 (20)

where N denotes the number of terms (vibration modes) considered,  $u_i(\tau)$  are the timedependent functions to be determined, and  $\phi_i(z)$  are the mode shapes of the cantilever beam. Increasing the number of terms generally leads to convergence of the ROM solutions [17]. However, a trade-off always exists between accuracy and computational cost. The differential equation of motion used for ROM is given by Eq. (2) after it is multiplied by  $(1-u)^2$ . The resulting  $(1-u)^{(7/9)}$  is expanded in Taylor series and terms up to the fifth power of u are retained, where  $\lambda_k$  are the Taylor polynomial coefficients. The resulting equation, using the Galerkin method, is multiplied by  $\phi_n$  and integrated from 0 to 1, resulting a system of N second order differential equations, n = 1, 2, ... N as follows

$$\begin{split} \sum_{i,j,k=1}^{N} \ddot{u}_{i}u_{j}u_{k}h_{nijk} - 2\sum_{i,j=1}^{N} \ddot{u}_{i}u_{j}h_{nij} + \sum_{i=1}^{N} \ddot{u}_{i}h_{ni} + \sum_{i,j,k=1}^{N} \omega_{i}^{2}u_{i}u_{j}u_{k}h_{nijk} \\ -2\sum_{i,j=1}^{N} \omega_{i}^{2}u_{i}u_{j}h_{nij} + \sum_{i=1}^{N} \omega_{i}^{2}u_{i}h_{ni} + b^{*}\sum_{i,j,k=1}^{N} \dot{u}_{i}u_{j}u_{k}h_{nijk} \\ -2b^{*}\sum_{i,j=1}^{N} \dot{u}_{i}u_{j}h_{nij} + b^{*}\sum_{i=1}^{N} \dot{u}_{i}h_{ni} = \delta V^{2}\{0.15h_{n} + C_{f}f^{*}[h_{n} - \lambda_{1}\sum_{i=1}^{N} u_{i}u_{j}h_{ni} - \lambda_{2}\sum_{i,j=1}^{N} u_{i}u_{j}h_{nij} - \lambda_{3}\sum_{i,j,k=1}^{N} u_{i}u_{j}u_{k}h_{nijk} - \lambda_{4}\sum_{i,j,k,l=1}^{N} u_{i}u_{j}u_{k}u_{l}h_{nijkl} - \lambda_{5}\sum_{i,j,k,l,m=1}^{N} u_{i}u_{j}u_{k}u_{l}u_{m}h_{nijkl}]\} \end{split}$$

where n = 1, 2, ..., N,  $h_{j_1 j_2 ... j_p} = \int_0^1 \phi_{j_1} \phi_{j_2} ... \phi_{j_p} dz$ , and  $\lambda_k$  are coefficients resulting from the ROM Taylor expansion. The numerical integration of 2T ROM and simulation of time responses of the cantilever beam are carried out using MATLAB [17]. AUTO-07p, a continuation and bifurcation software package, is utilized to solve Eq. (21) and predict the voltage-amplitude response [16, 17].

### 6 Results and Conclusions

Cantilever dimensionless mode shapes  $\phi_i(z)$ , and dimensionless natural frequencies  $\omega_k$ used in this research are given in Ref. [18]. Table 1 shows dimensional data of a typical MEMS resonator, and Table 2 the dimensionless parameters from Table 1 and Eq. (6). Figure 2 (left) shows the voltage–amplitude response of the capacitance model as predicted by the Method of Multiple Scales (MMS) and the two-term Reduced Order Model (2T ROM). The voltage parameter  $\delta$  is plotted on the x-axis, while Umax (the dimensionless deflection of the free end of the cantilever) is on the y-axis. MMS predicts three solutions: one of zero amplitude and two of non-zero amplitudes. They consist of stable and unstable branches. Solid lines represent stable solutions, while dashed lines indicate unstable ones. The MMS solution using a 5th-degree Taylor polynomial for the fringe electrostatic force in Eq. (10) shows a stronger softening effect, i.e. stronger bending to lower voltage values at larger amplitudes of the branches than the one using a 3rd-degree Taylor polynomial. This illustrates that including higher-order terms in the Taylor expansion within MMS yields more accurate results at large amplitudes. Bifurcation points A and B are subcritical and supercritical bifurcation points, respectively, C a saddle-node bifurcation point, and D end point of BD stable branch.

Parameter	Symbol	Value	Unit
Young's Modulus	E	169	GPa
Material Density	$\rho$	2330	kg/m <sup>3</sup>
Beam Length	l	300	μm
Beam Width	W	20	μm
Beam Thickness	h	2	μm
Initial Gap Distance	g	8	μm

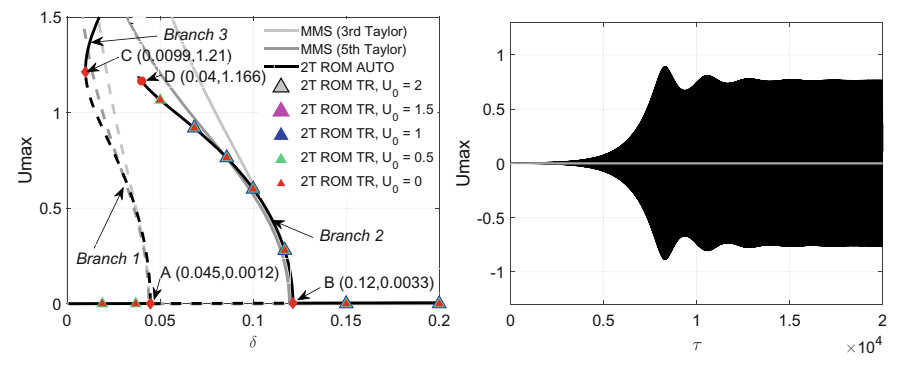
**Table 1.** Typical MEMS Cantilever Resonator Dimensional System Parameters

Figure 2 (right) shows a time response of the structure. One can notice the agreement between the time response and 2T ROM AUTO predictions.

Figure 3 (left) shows a comparison between the voltage responses at parametric resonance of the fringe capacitance model (CAP) based on Sakurai and Tamara [14] and the fringe model (F) based on Palmer formula [18, 19]. The capacitance model was modified to include only fringe contributions (i.e., the parallel-plate capacitance component is neglected). The fringe model based on Palmer's formula was also adjusted

Parameter	Symbol	Value
Voltage Parameter	δ	0.1
Damping Parameter	b	0.001
Fringe Parameter	f	0.26
Cap Fringe Parameter	$f^*$	0.29395

Table 2. Dimensionless System Parameters



**Fig. 2.** Capacitance model for  $b^* = 0.001$ , f = 0.26,  $f^* = 0.29395$ ,  $\sigma = -0.002282$ ,  $\omega_1 = 3.516015$ : (left) Voltage-amplitude response of parametric resonance of fringe electrostatically actuated MEMS cantilever resonator; (right) 2T ROM time response (TR) for initial amplitude  $U_0 = 0$  and  $\delta = 0.0858$ .

to exclude the parallel-plate capacitance, retaining only fringe field contributions. The main difference between the two models lies in the fringe contributions they consider. The capacitance model accounts for contributions from both the top and sidewalls of the beam, while the fringe model includes only the top surface contributions. The capacitance model exhibits a much narrower resonant zone (between A and B) compared to the fringe model while the bifurcation points are shifted toward significantly lower voltages. This is due to a larger fringe contribution in the capacitance model, thus requiring a smaller voltage parameter to induce a response. Notably, the capacitance model can also predict system behavior at amplitudes greater than the gap, a regime the fringe model fails to capture. Although the accuracy of the capacitance model's predictions at large amplitudes (e.g., branch 3) still needs verification, perhaps through the use of an alternative fringe capacitance equation, its ability to model behavior beyond the gap distance is significant. Given that this study focuses on system behavior at amplitudes greater than the gap between the cantilever and the ground plate, the capacitance model offers a substantial advantage over the fringe model. Finally, note that the detuning frequency selected for each voltage response must lie within the resonant zone of its corresponding frequency response. In this case, since the resonant zones of the capacitance and fringe models overlap slightly, the same detuning frequency was used for both voltage responses ( $\sigma_1$ 

= -0.002282). Underestimating or overestimating the fringe effect parameter can lead to instability for lower or larger voltages than anticipated.

Figure 3 (right) shows a comparison of voltage-amplitude responses of parametric resonance between capacitance model (Cap) in the case of ground plate with a hole and the Palmer formula model to include fringe effect (ES + F) in the case of a ground plate without a hole. Since the frequency response resonant zones of the capacitance and fringe models do not fall within the same resonant zone, two different detuning frequencies are used for this comparison,  $\sigma_1$  and  $\sigma_2$ . If the detuning frequency is not between the two bifurcation points subcritical and supercritical of the corresponding frequency response, then zero voltage response will be produced. Detuning frequency  $\sigma_1$  is for the capacitance (Cap) model while  $\sigma_2$  is for Palmer electrostatic + fringe (ES + F) case. So, a direct comparison between Cap and ES + F cannot be made.

However, one can notice that when compared to the ground plate without a hole modeled by Palmer (electrostatic + fringe) formula, the ground plate with a hole modeled by the capacitance model shows that: 1) the amplitudes are much larger going beyond the gap distance (Umax > 1) as the cantilever can deflect through the hole, 2) the voltage range between the subcritical and supercritical bifurcation points is lower, 3) the voltage of the supercritical bifurcation point is significantly lower. On should notice that for the ground plate without a hole the maximum deflection is the gap (Umax = 1) when the beam makes contact the ground plate, i.e. experiences a pull-in phenomenon.

Overall, comparing voltage responses due to different actuation models is significant in determining how adding fringe contributions affects the behavior of the system. Future work includes primary resonance [20] as well as NEMS [21, 22].

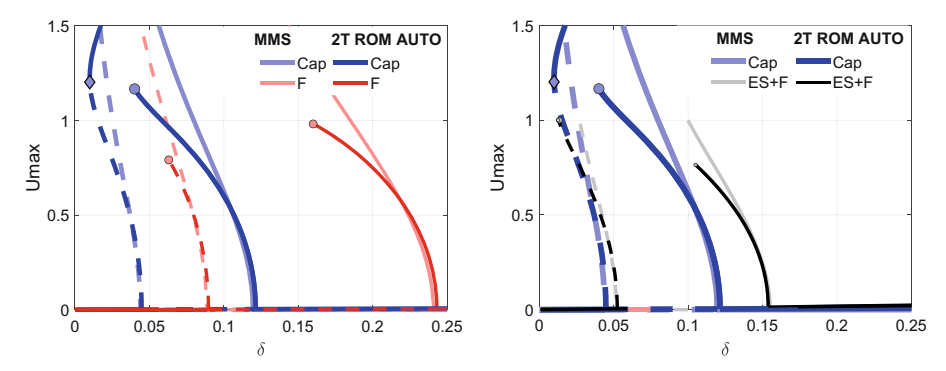


**Fig. 3.** Voltage-amplitude response of parametric resonance of fringe electrostatically actuated MEMS cantilever resonator  $b^* = 0.001, f = 0.26, f^* = 0.29395, \omega_1 = 3.516015$ . (left) Capacitance model versus fringe model for  $\sigma = -0.002282$ . (right) Ground plate with a hole, capacitance model,  $\sigma_1 = -0.002282$ , versus ground plate without a hole, Palmer formula (ES + F),  $\sigma_2 = -0.012475$ .

## References

- 1. Mayurika, J.B.: A review study on MEMS. J. Emerg. Technol. Innov. Res. 3(8), 748–753 (2016)
- Faudzi, A., Sabzehmeidani, Y., Suzumori, K.: Application of MEMS as sensors: a review. J. Robot. Mechatron. 32(2), 281–288 (2020)

- Ghazali, A.A., et al.: A review of actuation and sensing mechanisms in MEMS-based sensor devices. Nanoscale Res. Lett. 16(16), 1–21 (2021)
- 4. Nazir, S., Kwon, O.: Micro-electromechanical systems-based sensors and their applications. Appl. Sci. Converg. Technol. **31**(2), 40–45 (2022)
- 5. Chircov, C., Grumezescu, A.M.: Microelectromechanical systems (MEMS) for biomedical applications. Micromachines **13**(2), 1–31 (2022)
- 6. Pujol-Villa, F., Villa, R., Alvarez, M.: Nanomechanical sensors as a tool for bacteria detection and antibiotic susceptibility testing. Front. Mech. Eng. **6**(44), 1–18 (2020)
- 7. Ilic, B., Czaplewski, D., Craighead, H.G., Neuzil, P., Campagnolo, C., Batt, C.: Mechanical resonant immunospecific biological detector. Appl. Phys. Lett. **77**(3), 450–452 (2000)
- 8. Batra, R.C., Porfiri, M., Spinello, D.: Capacitance estimate for electrostatically actuated narrow microbeams. Micro Nano Lett. 1(2), 71–73 (2007)
- 9. Liu, X., Zhang, L., Zhang, M.: Studies on pull-in instability of an electrostatic MEMS actuator: dynamical system approach. J. Appl. Anal. Comput. **12**(2), 850–861 (2022)
- Van der Meijs, N.P., Fokkema, J.T.: VLSI circuit reconstruction from mask topology. Integr. VLSI J. 2, 93–98 (1984)
- 11. Krakover, N., Ilic, B.R., Krylov, S.: Micromechanical resonant cantilever sensor actuated by fringing electrostatic fields. J. Micromech. Microeng. **32**, 054001 (2022)
- 12. Krakover, N., Ilic, B.R., Krylov, S.: Resonant pressure sensing using a micromechanical cantilever actuated by fringing electrostatic fields. In: 2018 Proc. IEEE Int. Conf. Micro Electro Mech. Syst. (MEMS), pp. 846–849 (2018)
- 13. Chang, W.H.: Analytical IC metal-line capacitance formulas. IEEE Trans. Microw. Theory Techn., 608–611 (1976)
- Sakurai, T., Tamaru, K.: Simple formulas for two- and three-dimensional capacitances. IEEE Trans. Electron Devices 30(2), 183–185 (1983)
- 15. Moran, K., Burgner, C., Shaw, S., Turner, K.: A review of parametric resonance in micro electromechanical systems. IEICE Nonlinear Theory Appl. 4(3), 198–224 (2013)
- Caruntu, D.I., Martinez, I., Knecht, M.W.: Parametric resonance voltage response of electrostatically actuated micro-electro-mechanical systems cantilever resonators. J. Sound Vib. 362, 203–213 (2016)
- Caruntu, D.I., Juarez, E.: Coaxial vibrations of electrostatically actuated DWCNT resonators: amplitude-voltage response of parametric resonance. Int. J. Non-Linear Mech. 142, 103982 (2022)
- Caruntu, D.I., Knecht, M.W.: Microelectromechanical systems cantilever resonators under soft alternating current voltage of frequency near natural frequency. J. Dyn. Syst. Meas. Control 137, 041016 (2015)
- 19. Palmer, H.B.: The capacitance of a parallel-plate capacitor by the Schwartz-Christoffel transformation. Trans. AIEE **56**(3), 363–366 (1937)
- Caruntu, D.I., Martinez, I., Taylor, K.I.: Voltage-amplitude response of alternating current near half natural frequency of electrostatically actuated MEMS resonators. Mech. Res. Commun. 52, 25–31 (2013)
- Caruntu D.I., Reyes C.A.: Casimir effect on amplitude-frequency response of parametric resonance of electrostatically actuated NEMS cantilever resonators. In: Chapter 15 in Developments and Novel Approaches in Biomechanics and Metamaterials. Series: Adv. Struct. Mater., vol. 132, pp. 267–289. Springer, Cham (2020)
- 22. Caruntu, D.I., Beatriz, J.S.: Quantum dynamics effects on amplitude-frequency response of superharmonic resonance of second-order of electrostatically actuated NEMS circular plates. In: Chapter 4 in Theoretical Analyses, Computations, and Experiments of Multiscale Materials, Series: Adv. Struct. Mater., pp. 69–104. Springer, Cham (2022)